Novel Multifunctional Optical-Fiber Probe: II. High-Density CFB Measurements

Jinzhong Liu, John R. Grace, and Xiaotao Bi
Dept. of Chemical and Biological Engineering, The University of British Columbia, Vancouver, Canada V6T 1Z4

The novel parallel three-fiber optical probe described in Part I of this article is applied to determine simultaneously local instantaneous solids volume concentration, velocity, and flux in multiphase suspensions. Radial distributions of local particle concentration, velocity, and flux and their fluctuations in a high-density circulating fluidized bed (HDCFB) are presented. A strong correlation exists between fluctuations of local particle velocity and particle concentration. The optical probe is shown to provide a means of evaluating alternative measurement techniques that have commonly been employed in earlier studies.

Introduction

Due to the limitations of experimental equipment and techniques, very few studies have been conducted on the radial distribution of particle velocities in high-density circulating fluidized beds with solids circulation fluxes beyond ~200 kg/m^2·s. Part I of this article (Liu et al.) describes a newly developed optical-fiber probe capable of providing simultaneous measurements of particle concentration, particle velocity, and solids flux in flowing fluid–solid suspensions covering a wide range of conditions. In this article we present experimental results showing instantaneous local voidage, particle velocity, and solids flux, determined simultaneously in a high-density circulating fluidized-bed (CFB) riser.

Experimental Details

The multifunctional optical-fiber probe presented in detail in Part I was inserted into a high-density CFB riser of diameter 76 mm and total height 6.4 m at different levels from the bottom J-valve to the exit. FCC particles of mean diameter 70 μm and density 1,600 kg/m^3 were used. The high-density CFB riser unit is shown in Figure 1.

At each level, measurements were performed at different radial positions from the near wall to the opposite wall. Apparent solids holdups were also obtained using differential- and absolute-pressure transducers to compare with average cross-sectional values estimated by integrating local solids holdups measured by the optical probe at different radial positions.

Criteria to judge whether or not the cross-correlated velocity data are valid (see Part I) were applied in each case. This eliminated some data points. Almost 100% of the cross-correlated velocities were accepted in the central region ($|r/R| < 0.8$), while up to 40% of the data were eliminated near the wall ($r/R = 0.95$). The average cross-correlation coefficients were much higher in the central region than near the wall, probably due to more particles traveling nonvertically and to particles reversing directions in the wall region. Figure 2 shows the accepted cross-correlation coefficients for a typical operating condition. At $r/R = 0.5$, the average cross-correlation coefficient was about 0.98, while it was only 0.87 near the wall ($r/R = 0.9$) for all accepted data points.

Figure 3 plots typical traces of instantaneous local solids holdup ($1 - \epsilon$), local particle velocity (v_p), and local solids flux ($G_s(t)$), obtained by the optical-fiber probe vs. time. Each velocity point was obtained off-line by cross-correlating 4,096 binary voltage data from the two channels (channels 1 and 2) over an integration period of T (see Part I). The corresponding solids volume fraction was obtained by averaging over the same duration, T, the time for each channel to load 4,096 binary data, ~14.6 ms at a sampling frequency of ~280 kHz, except in the wall region ($r/R \geq 0.95$), where $T \approx 40$ ms for a sampling frequency of 180 kHz. The fluctuations reflect rapid changes in suspension density, particle velocity, and local flux. Averaging such data over the overall measurement duration (20 to 40 s) gives time–mean local values of local solids

Correspondence concerning this article should be addressed to J. R. Grace.

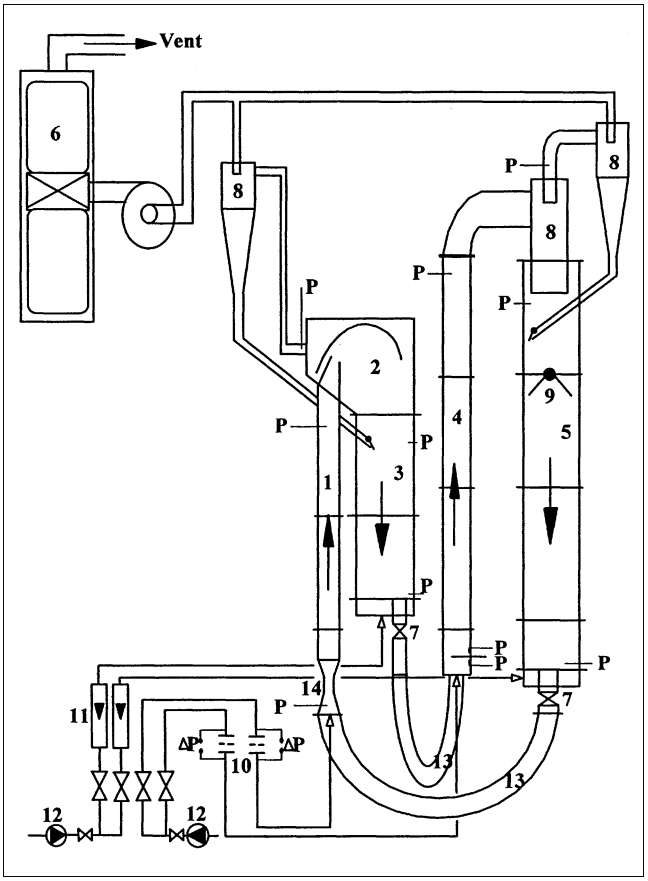

Figure 1. High-density CFB unit.

1. First riser; 2. impingement separator; 3. storage tank; 4. second riser; 5. downcomer; 6. baghouse; 7. pinch valve; 8. cyclone; 9. butterfly valve; 10. orifice meter; 11. rotameter; 12. Root's blower; 13. J-valve; 14. venturi section; P—absolute pressure transducer port; ΔP—manometer.

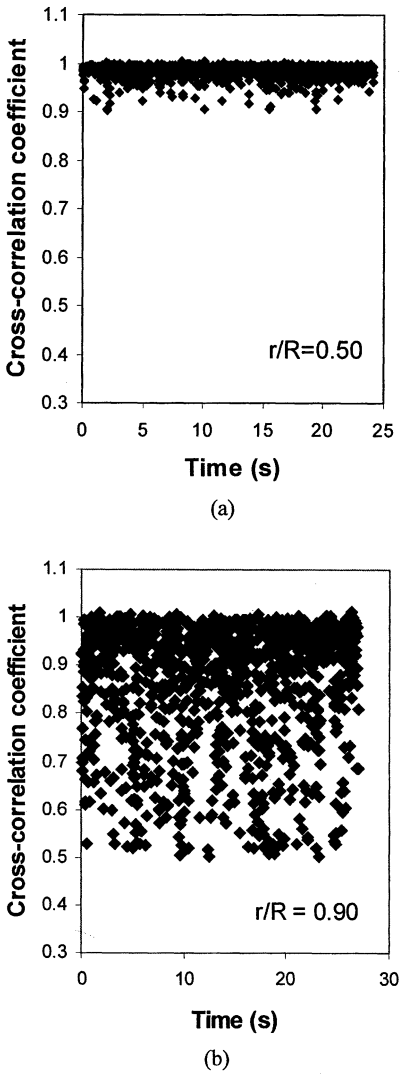

Figure 2. Cross-correlation coefficients for $U_g = 4.0$ m/s, $G_{sm} = 325$ kg/m^2·s, and $z = 4.2$ m.

holdup, particle velocity, and solids flux, that is

$$\bar{c} = 1 - \bar{\epsilon} = \frac{1}{T}\int_0^T ((1-\epsilon)(t))\, dt = \frac{1}{N}\sum_{i=1}^{N}(1-\epsilon_i) = \frac{1}{N}\sum_{i=1}^{N} c_i \tag{1}$$

$$\overline{v_p} = \frac{1}{T}\int_0^T \big(v_p(t)\big)\, dt = \frac{1}{N}\sum_{i=1}^{N} v_{p_i} \tag{2}$$

$$\overline{G_s} = \frac{1}{T}\int_0^T \big(G_s(t)\big)\, dt = \frac{1}{N}\sum_{i=1}^{N} G_{s_i} \tag{3}$$

The instantaneous velocity and concentration can also be written as

$$1 - \epsilon = (1 - \bar{\epsilon}) - \epsilon' \quad \text{or} \quad c = \bar{c} + c' \tag{4}$$

$$v_p = \overline{v_p} + v_p', \tag{5}$$

where the primes denote fluctuating components. Considering the relationship between the three instantaneous parameters

$$G_s = \rho_p(1-\epsilon)v_p = \rho_p(\bar{c} + c')\big(\overline{v_p} + v_p'\big) \tag{6}$$

Combining Eqs. 3–6, and averaging leads to

$$\overline{G_s} = \rho_p\big(\overline{cv_p} + \overline{c'v_p'}\big). \tag{7}$$

The final term of this equation indicates that the covariance of particle velocity and concentration can play an important role, as discussed in the next section.

Cross-sectional mean values are obtained by integrating the local time–mean variables over the column cross-sectional area, that is

$$c_m = 1 - \epsilon_m = \int_0^1 2(1-\bar{\epsilon})\varphi\, d\varphi \tag{8}$$

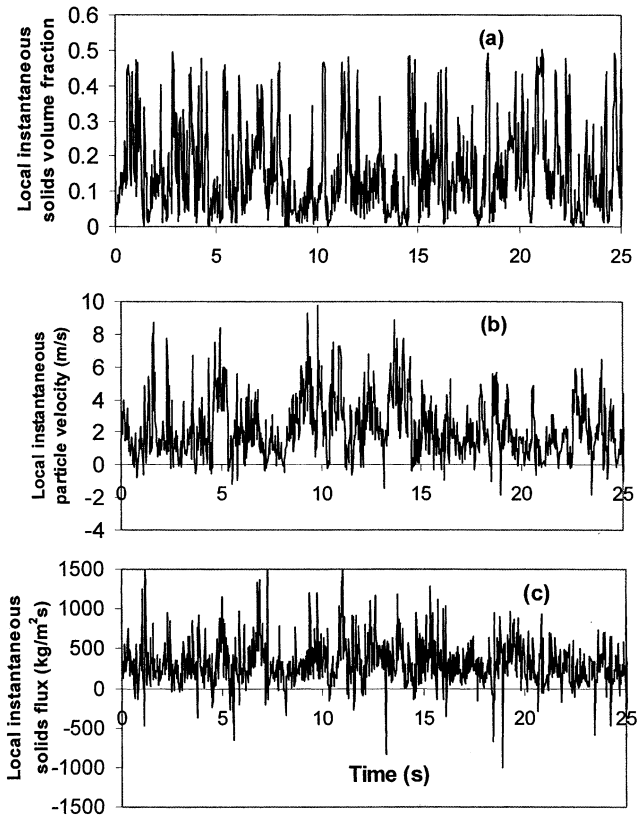

Figure 3. Local instantaneous (a) solids holdup, (b) particle velocity, and (c) solids flux vs. time.

$r/R = 0.74$, $z = 4.2$ m, $U_g = 9$ m/s, $G_{sm} = 485$ kg/m^2·s, and the same 25 s time interval.

$$G_{sm} = \int_0^1 2\overline{G_s}\varphi \, d\varphi, \tag{9}$$

where $\varphi = r/R$.

Typical radial profiles of the local time–mean vertical component of particle velocity, solids holdup, and solids flux based on Eqs. 1–3 at $z = 4.2$ m for high-density operation ($U_g = 4.0$ m/s, $G_s = 325$ kg/m^2·s) appear in Figure 4. For this particular operating condition, the radial particle velocity profile is bell-shaped, with a maximum at the axis and decreasing toward the wall. The corresponding solids holdup profile is bathtub shaped, remaining relatively flat over a considerable radial distance before increasing sharply near the wall, forming a dilute central core and a dense wall region, as reported by Issangya et al. (2000). The corresponding solids flux profile is again relatively uniform in the central region, then decreases quickly toward the riser walls.

Ideally, the radial profiles should be axisymmetric, especially well above the distributor ($z = 4.2$ m) and well (2.1 m) below the riser exit. Figure 4 indicates an approximately symmetric profile of the particle velocity. However, the measured solids concentrations on the left side are appreciably higher than on the right side, resulting in higher solids fluxes on the left. Because the probe on the left side of the riser is less intrusive, and therefore likely to be more accurate than on the right, the results on the lefthand side have been used to obtain cross-sectional average values, assuming axisymmetric profiles.

Fluctuations of Local Particle Velocity, Concentration, and Flux

Fluctuations in the instantaneous local variables—particle concentration, velocity, and flux—reflect turbulence of the local suspension flow. The standard deviation of particle flux is related to the turbulent intensity and is a key parameter in modeling the suspension flow. Our probe allows determination of the instantaneous particle fluxes and their fluctuations.

Local solids holdup fluctuations are shown in Figure 5 with corresponding probability distributions at five radial positions for $z = 4.2$ m, $U_g = 8$ m/s, and a net solids circulation flux of 455 kg/m^2·s. The local voidage traces and corresponding probability distributions are similar to those reported by Is-

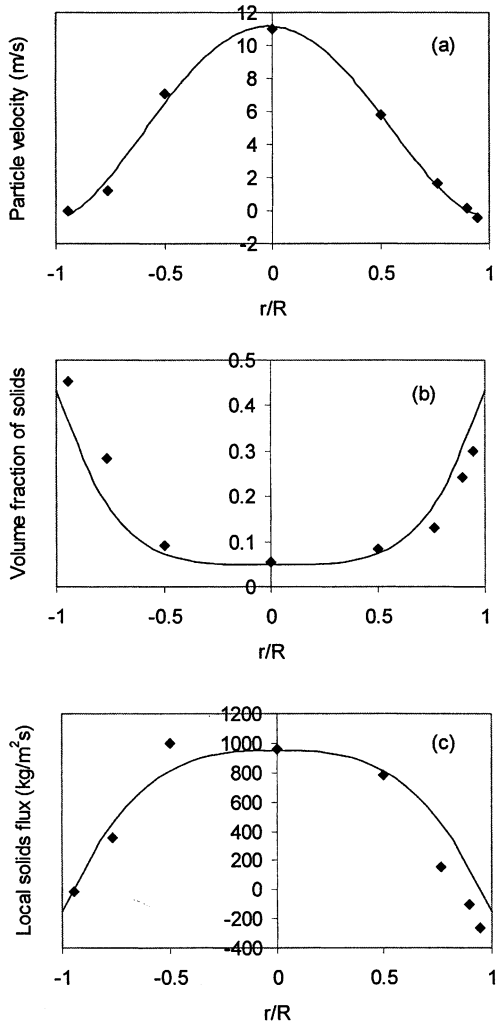

Figure 4. Radial profiles of (a) time-average local solids velocity, (b) time-average local solids concentration, and (c) time-average local solids flux.

$U_g = 4.0$ m/s, $G_{sm} = 325$ kg/m^2·s, $z = 4.2$ m.

sangya et al. (2000), based on a multifiber optical probe that only measured particle concentration.

Figure 6 shows traces of instantaneous particle velocity for the same operating conditions as in Figure 5. The cross-sectional mean solids holdup is 0.17, a typical value for high-density conditions. The corresponding probability distributions for the whole measurement period are also included in Figure 5. In the dilute central region of the riser, the particle velocity is high and accompanied by high-amplitude fluctuations, coupled with low-amplitude fluctuations of solids volume fraction. The corresponding probability distribution of particle velocity in this region is relatively wide, indicating large fluctuations and strong turbulence, while the corresponding probability distribution of solids holdup gives a narrow peak, showing a relatively homogeneous dilute suspension flow at the axis. Further outward, the fluctuations in lo-

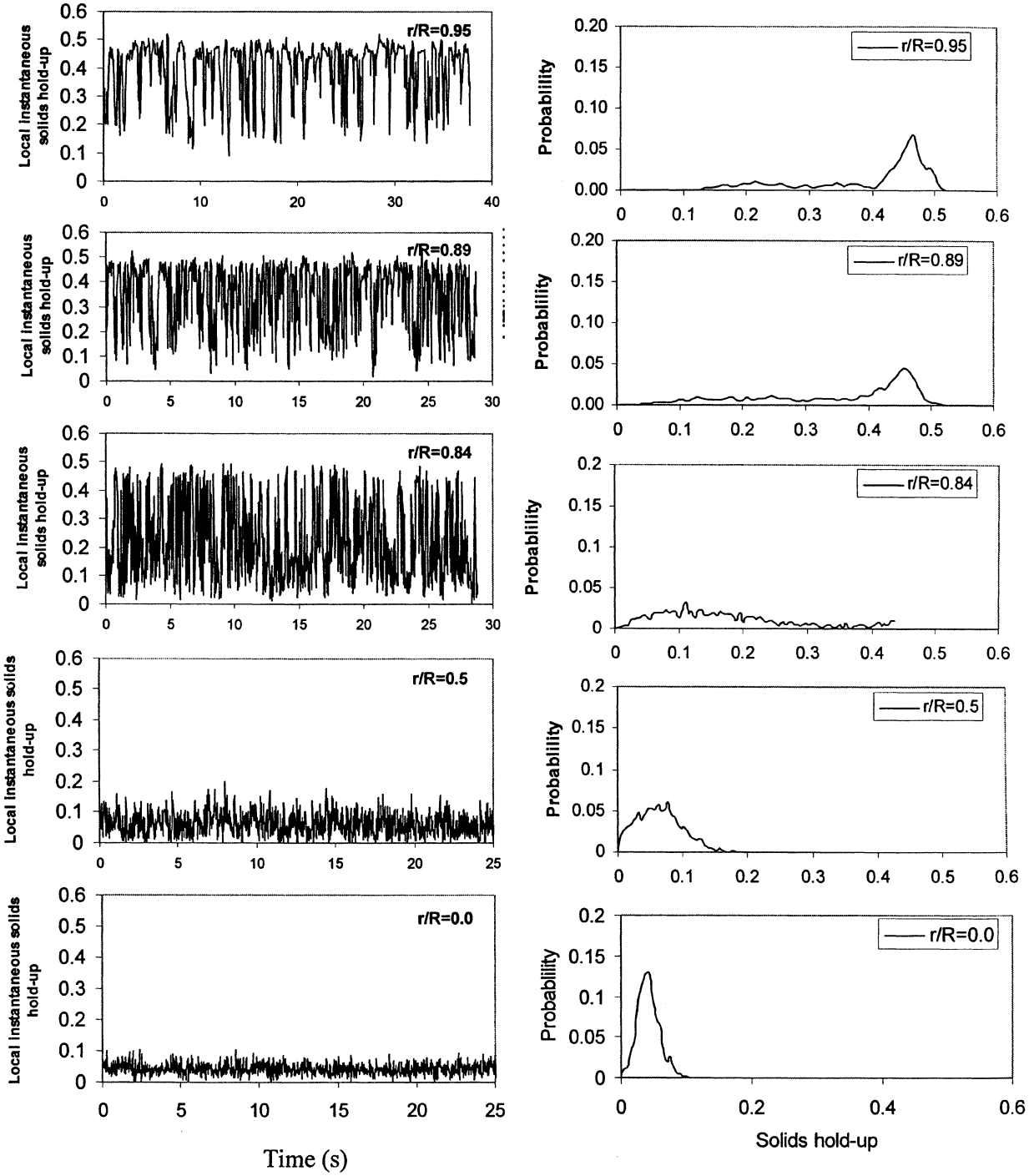

Figure 5. Local solids holdup vs. time with corresponding probability distribution plots for five radial locations.

U_g = 8 m/s, G_{sm} = 455 kg/m^2·s, and z = 4.2 m. Cross-sectional average solid volume fraction = 0.17, obtained by integration of local holdups.

cal particle velocity tend to be weaker and less frequent, with a narrower probability distribution. At the same time, the average local particle velocity shifts to smaller magnitudes, while the suspension becomes denser toward the wall. The most frequently encountered particle velocity at $r/R = 0.95$ is negative. However, as discussed by Bi et al. (1996), this does not necessarily indicate that the net flow direction is downwards. No previous researchers have reported continuous local particle velocity traces.

The new probe enables local instantaneous fluxes to be determined. Figure 7 plots local instantaneous solids fluxes for the same operating condition as in Figures 5 and 6. The cor-

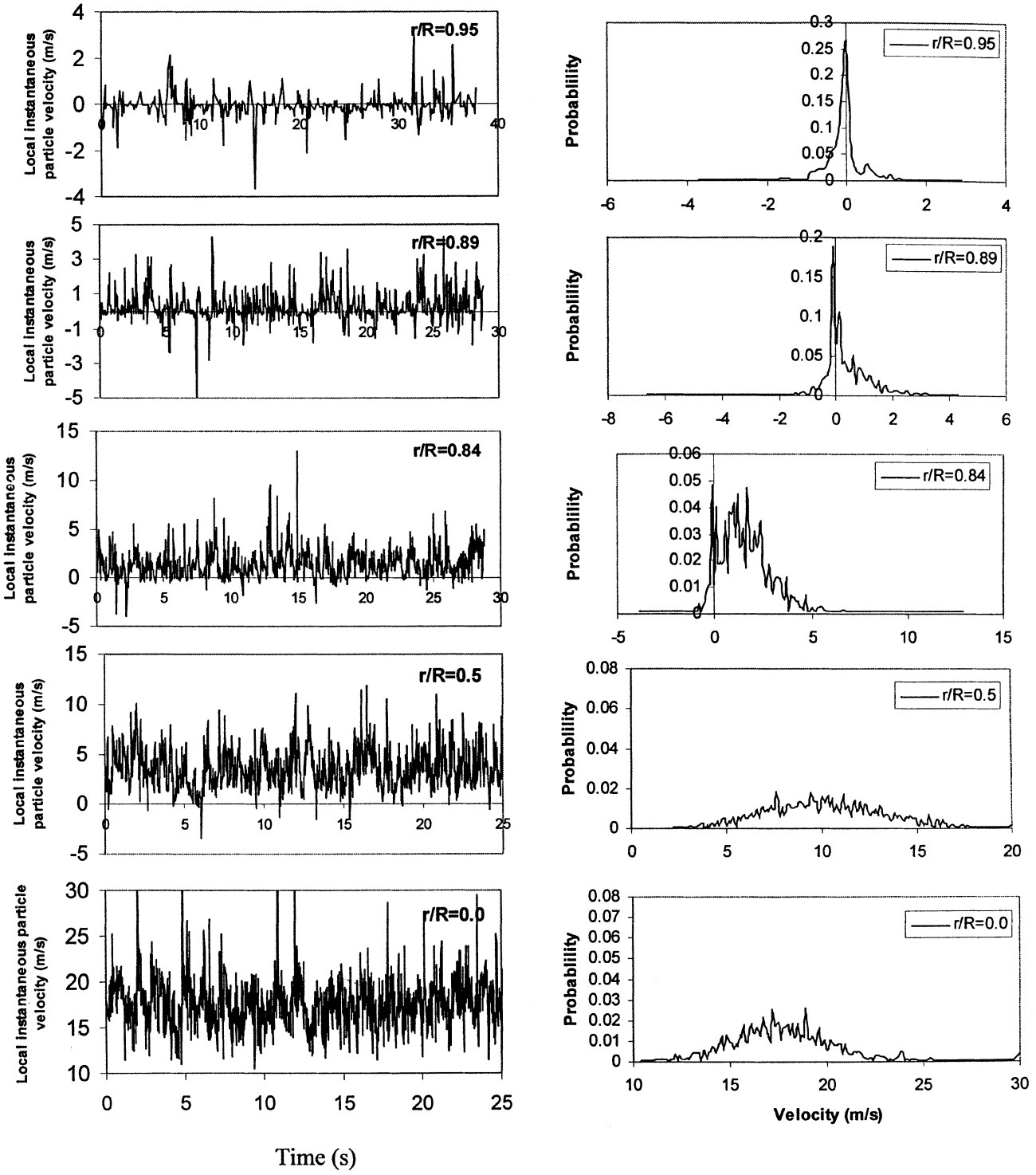

Figure 6. Local velocity vs. time with the corresponding probability distribution plots at five radial locations.

$U_g = 8$ m/s, $G_{sm} = 455$ kg/m^2·s, and $z = 4.2$ m.

responding probability distributions are also included for the same measurement periods. In the dilute central region of the riser, all solids fluxes are positive, fluctuating over a wide range. This range "shifts" toward the negative side and becomes narrower as the probe is traversed toward the wall. Finally, the time–mean value falls below zero, with instantaneous values mostly between -500 and 500 kg/m^2·s, as seen from the probability distributions.

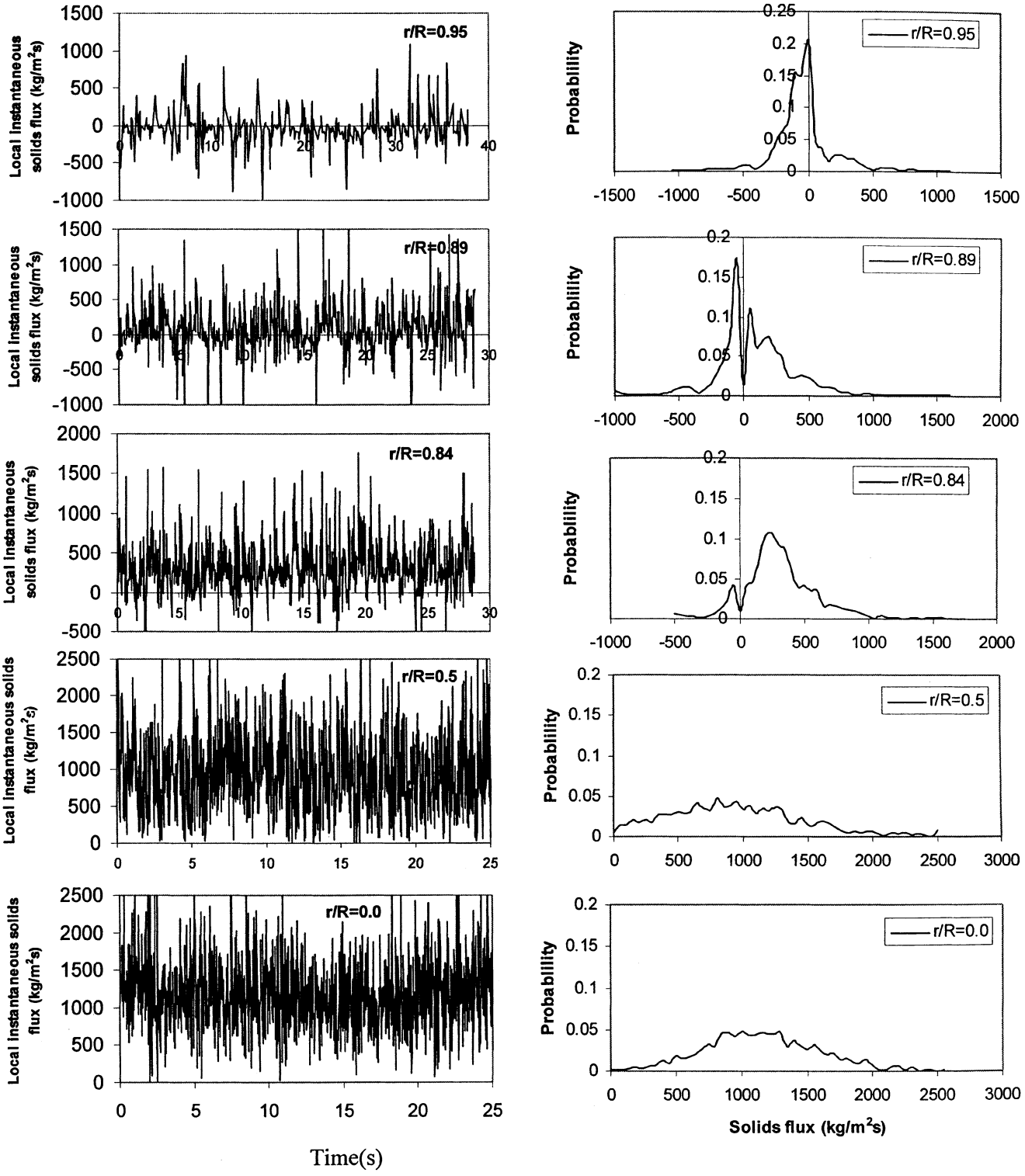

Figure 7. Local solids flux vs. time with the corresponding probability distributions for five radial locations.

$U_g = 8$ m/s, $G_{sm} = 455$ kg/m^2·s, and $z = 4.2$ m.

Fluctuations of local solids flux are closely related to the distributions of instantaneous solids concentration (Figure 5) and velocity (Figure 6). Because both the particle velocity and its fluctuations are high at the center, the solids flux is high with high-amplitude fluctuations in this region. The corresponding probability distribution is wide, indicating large fluctuations. Further outward, the fluctuations in local solids flux are weaker and less frequent. At the same time, the average local solids flux decreases with increasing r/R, while the suspension becomes denser and travels more slowly.

Relationship between Instantaneous Particle Concentration, Velocity, and Flux

Local instantaneous particle fluxes are closely related to particle velocity and solids volume fraction as shown by Eq. 6. Bi et al. (1996) noted, based on a theoretical analysis, that due to interaction between local particle velocity fluctuations and solids concentration fluctuations, the time–mean particle flux and velocity do not pass through zero at the same radial position. As a result, different annular wall layer thicknesses are obtained in the fast fluidization flow regime based on radial profiles of solids flux and radial profiles of particle velocity.

Unless fluctuations in velocity and concentration are uncorrelated, it is incorrect to ignore the second term on the righthand side of Eq. 7, that is, to assume that the product of local time–mean particle velocity and time–mean concentration gives the local time–mean solids flux. Since in general

$$\overline{G_s} \neq \rho_p \bar{c} \overline{v_p} \quad \text{or} \quad \overline{G_s} \neq \rho_p (1-\bar{\epsilon}) \overline{v_p}, \tag{10}$$

it is not appropriate to obtain the third of the three time–mean quantities $(\overline{G_s}, \bar{c}, \overline{v_p})$ or $(\overline{G_s}, \bar{\epsilon}, \overline{v_p})$ from the other two. Zhu et al. (1991) measured the time-varying particle density and mass-flow rate in a horizontal glass pipe of 51 mm ID for dilute suspensions (< 5 kg/m^3) of 200-μm glass beads in air. They found that the covariance of the density and velocity fields was $\sim$1 to 10% of the mass-flow rate and always negative, so that the product of time–mean density and velocity always overestimated the actual mass flow. Qian and Li (1994) reported a considerable difference between the direct time-average particle velocity and the weighted time-average with respect to bed density for FCC risers at $U_g = 2.5$ m/s and $G_s = 62$ kg/m^2·s. However, the first of these two groups applied an indirect measurement technique based on electrostatics to determine the mass flow, while the second applied a Pitot tube to measure the particle velocity, which is not well suited to determine instantaneous velocities.

Figure 8 plots the instantaneous particle velocity against the instantaneous solids concentration determined simultaneously by our multifunctional optical probe. At the axis, the instantaneous particle velocities and the corresponding solids concentrations appear to be uncorrelated. For the next three radial positions ($r/R = 0.5$, 0.84, and 0.89), a strong correlation can be identified, with higher solids holdup (such as due to streamers) usually corresponding to reduced velocities, while dilute structures mostly correspond to faster ascent. Near the wall, due to more solids descending and the more random flow structure, this trend is less obvious for the high flux conditions.

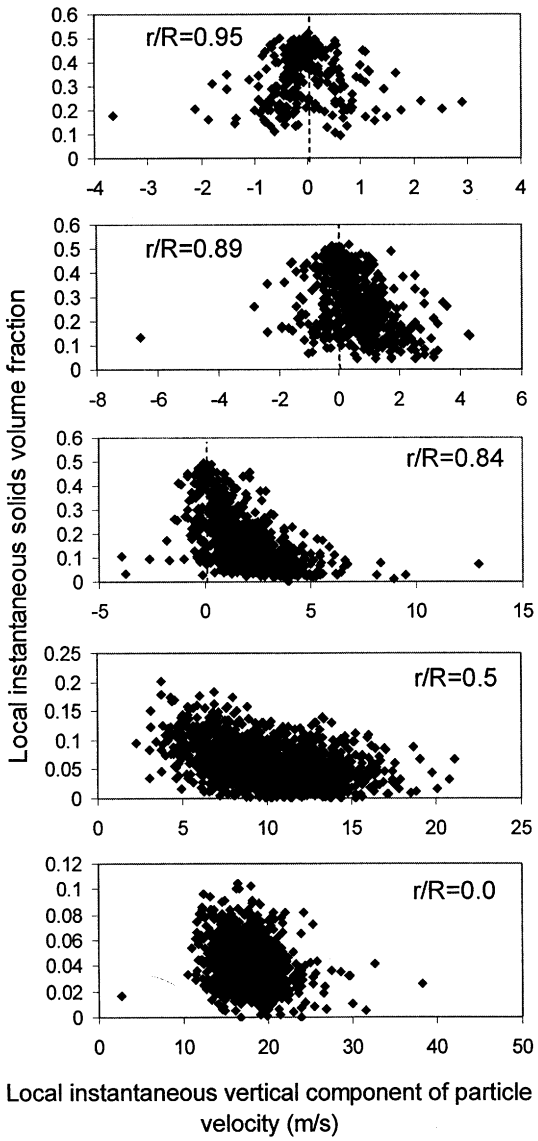

Figure 8. Local instantaneous vertical component of particle velocity vs. simultaneously measured local instantaneous solids concentration.

$U_g = 8.0$ m/s, $G_{sm} = 455$ kg/m^2·s, and $z = 4.2$ m.

The correlation between instantaneous particle velocity and concentration confirms that the average solids flux should not be obtained from the product of the time–mean solids concentration and the time–mean velocity. For convenience, we consider a normalized error factor

$$\Phi_{\text{Err}} = \frac{\rho_p (1-\bar{\epsilon}) \overline{v_p} - \overline{G_s}}{G_{sm}}, \tag{11}$$

where $1-\bar{\epsilon}$ and $\overline{v_p}$ are the local time–mean average solids volume fraction and particle velocity calculated from Eqs. 1 and 2, $\overline{G_s}$ is obtained by averaging the local instantaneous local fluxes over the same measurement duration as $(1-\epsilon)$ and (v_p), while G_{sm} is the integrated solids circulation flux over the whole cross section (i.e., Eq. 9).

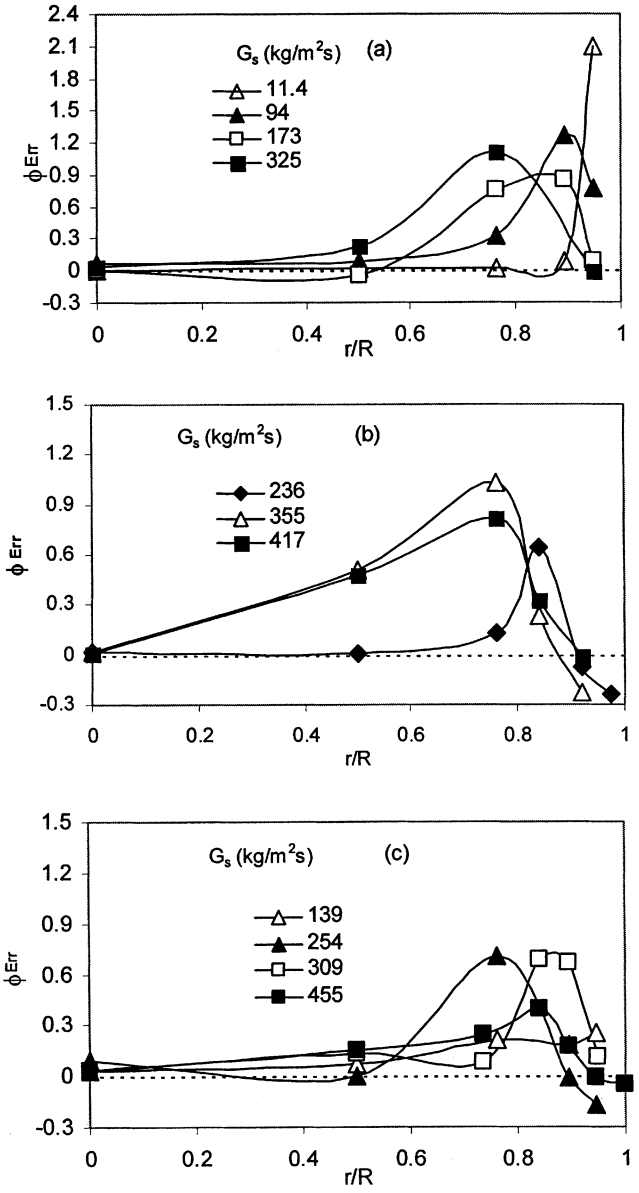

Figure 9. Radial profiles of error when time–mean solids flux is estimated by multiplying time–mean particle velocity by time–mean local suspension density at $z = 4.2$ m: (a) $U_g = 4$ m/s; (b) $U_g = 6$ m/s; (c) $U_g = 8$ m/s.

With the aid of Eq. 7, Eq. 11 can be rearranged to give

$$\Phi_{\mathrm{Err}} = -\frac{\rho_p \overline{c' v_p'}}{G_{sm}} = -\frac{\rho_p}{N G_{sm}} \sum_{i=1}^{N} (1 - \epsilon_i') v_{pi}' \qquad (12)$$

Therefore Φ_{Err} is simply the negative value of time–mean normalized covariance of suspension density and particle velocity.

Figure 9 plots radial profiles of Φ_{Err} for various operating conditions. In most cases, Φ_{Err} is positive, that is, the covariance between the two is negative and the particle velocity and concentration are negatively correlated. Positive correla-

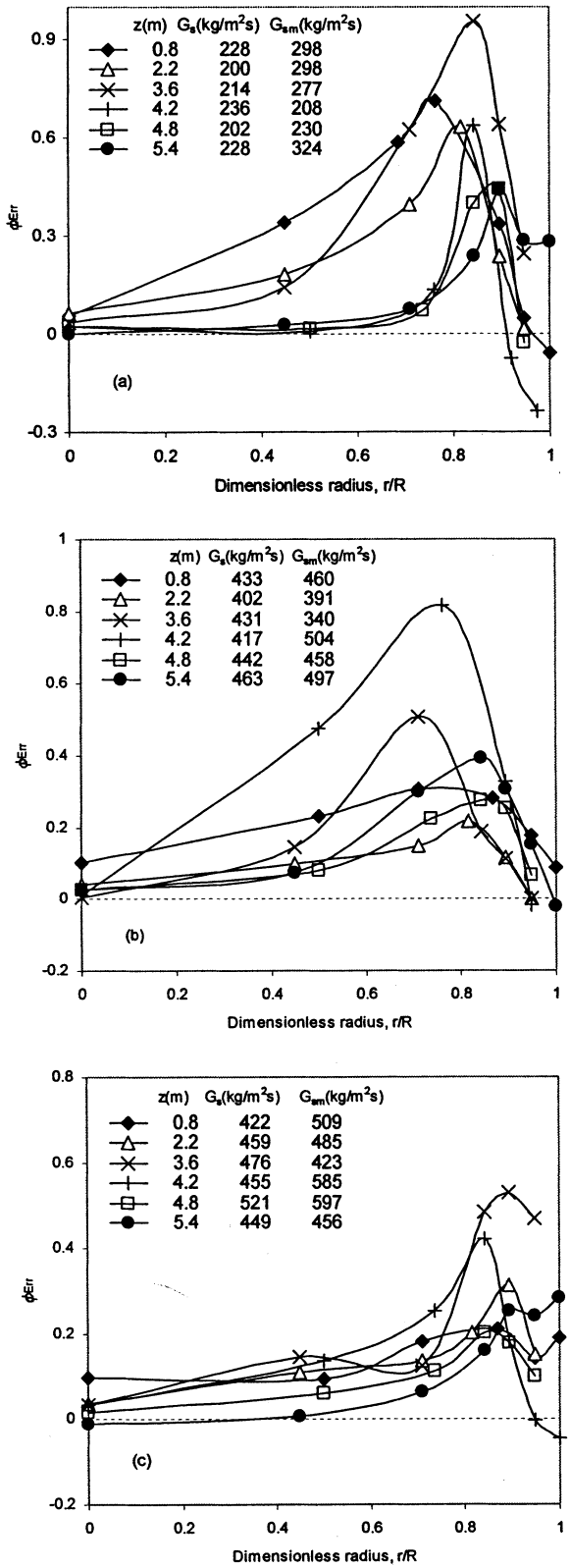

Figure 10. Radial profiles of dimensionless error when time–mean solids flux is estimated by multiplying time–mean particle velocity by time–mean local suspension density for: (a) $U_g = 6$ m/s; (b) $U_g = 6$ m/s; (c) $U_g = 8$ m/s.

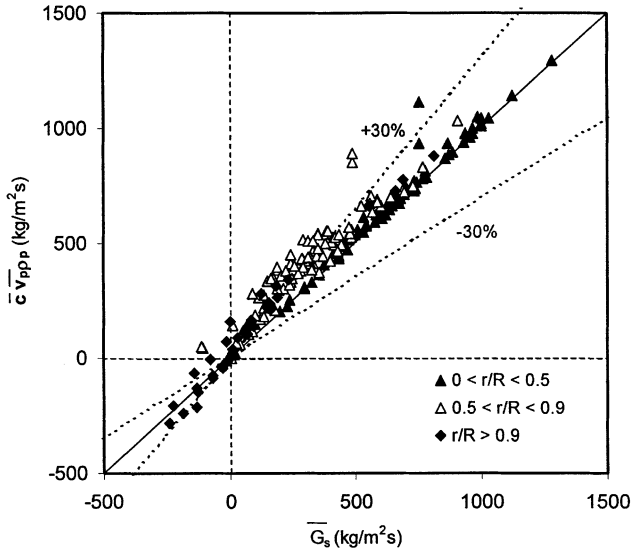

Figure 11. Products of time–mean particle velocity and the time–mean local suspension density vs. time–mean local solids fluxes.

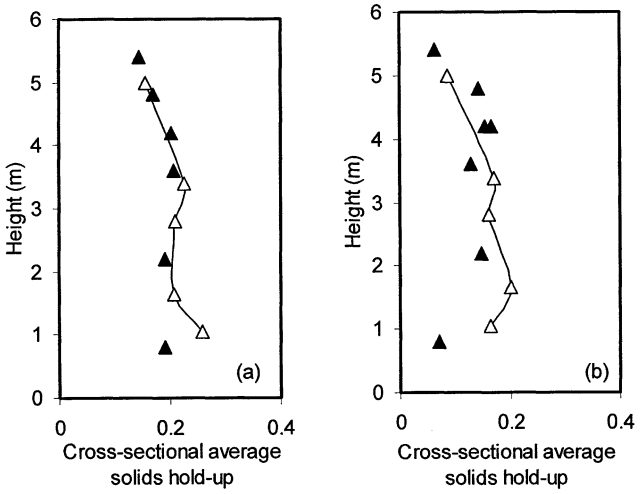

Figure 12. Comparison of axial solids holdup profiles obtained by optical-fiber probe and pressure transducers.

(a) U_g = 6 m/s, G_{sm} = 431 kg/m^2·s; (b) U_g = 8 m/s, G_{sm} = 453 kg/m^2·s. Open symbols were obtained by pressure transducers; closed symbols by optical-probe.

tion between the two parameters only occurs near the wall where both the net flow direction and particle velocity tend to be downwards. Multiplying the time–mean velocity by the time–mean suspension density overestimates the local solids flux in most cases. At the riser axis, the error is very small. Φ_{Err} then increases with r/R, reaches a peak, and falls to zero or a negative value at the wall. The maximum errors occur in the interior of the column, for example, at $r/R \approx 0.7 \sim 0.9$, where estimation of $\overline{G_s}$ based on $\rho_p \bar{c}\bar{v}_p$ causes the local solids flux to be overestimated by 50% to over 100%. Using the product of time–mean velocity and time–mean density to estimate the time–mean local solids flux is acceptable only at the riser axis. The error appears to be more significant at lower U_g.

The effect of height on the radial profiles of Φ_{Err} can be seen in Figure 10. The greatest negative covariances occur in the middle of the riser, that is, $z \approx 3.6 - 4.2$ m. This trend is somewhat similar to the axial profiles of radial particle velocity and flux distribution, suggesting that stronger radial nonuniformity corresponds to stronger correlation between the particle velocity and concentration.

Figure 11 plots local time–mean solids fluxes compared with those estimated by multiplying the local time–mean suspension density and particle velocity. It confirms that at very high solids fluxes (usually near the riser axis) and at very low fluxes (usually near the riser wall), the difference is relatively small. In the intermediate range, between the riser center and wall, the error is much larger. It also shows that multiplying the time–mean velocity by the time–mean suspension density almost always results in a larger magnitude than the true local solids flux.

The radial profile of particle velocity–concentration covariance can also be related to the radial transfer of particles. Jiang and Fan (1999) reported that the maximum radial transfer rates (radial solids fluxes) occurred between the riser center and wall. Earlier work by Qi and Farag (1993) showed a similar radial distribution of radial particle momentum exchange. The coincidence between the location of the maximum vertical velocity–concentration covariance and the radial transfer of particles indicates that turbulence is strongest at this location, this also being the region of strongest particle–particle collisions.

Further Evaluation of Optical-Fiber Probe

To further validate the novel optical probe, the measurement results are compared in this section with those obtained by other techniques, namely, pressure transducers to measure apparent solids holdups, the butterfly-valve quick-closing technique to measure total solids circulation rates (G_s), and a nonisokinetic sampling method to measure local time–mean solids flux. This comparison also provides an indication of the accuracy of these three relatively simple measurement techniques commonly applied in CFB systems.

Pressure transducers

The apparent solids holdups at superficial gas velocities of 6 and 8 m/s and high solids circulation fluxes (>400 kg/m^2·s) have been estimated from time-average differential pressures across sections of the riser by applying Eq. 20 of Part I, neglecting wall friction and solids acceleration/deceleration. In Figure 12 they are compared with the cross-sectional mean solids holdup values at different riser heights, obtained by integrating the local time–mean solids holdups measured by the dual-functional optical-fiber probe over the cross section, that is, Eq. 8. Note that due to a venturi section at the bottom section of the riser (see Figure 1), there is a particle deceleration zone in the lower part of the riser. Figure 12 shows reasonably good agreement between the two methods for most of the riser, excluding the inlet section. This helps to validate the use of the optical-fiber probe to measure solids

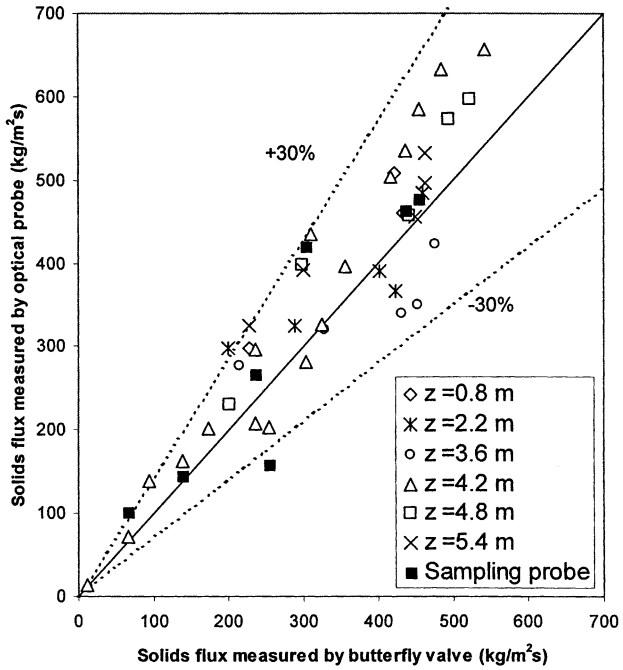

Figure 13. Comparison of solids circulation fluxes obtained by optical probe, nonisokinetic sampling probe, and butterfly-valve method for different operating conditions and heights.

All symbols except ■ are for optical-probe measurements.

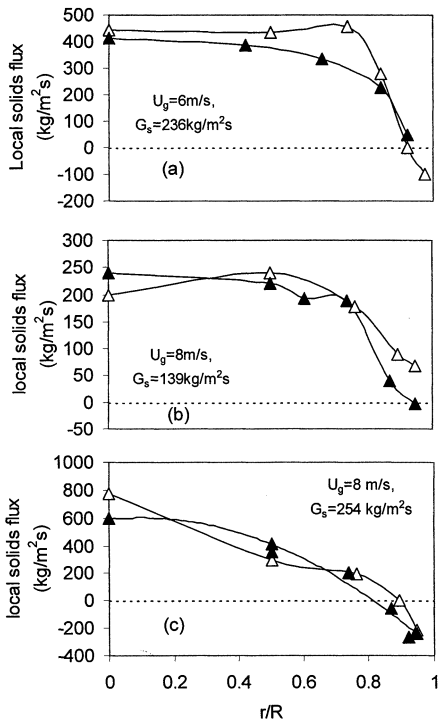

Figure 14. Comparison of radial profiles of local solids flux obtained by optical-fiber probe and nonisokinetic sampling probe at $z = 4.2$ m and various intermediate-density operating conditions.

Open symbols correspond to optical probe; closed symbols to suction probe.

concentration, given that the pressure gradient method has been separately validated (Arena et al., 1988), although it can lead to some error in the lower region of risers where neglect of the acceleration term is not fully justified (Weinstein and Li, 1989; Louge and Chang, 1990; Issangya, 1998).

Butterfly-valve quick-closing method

Figure 13 compares the integrated solids fluxes, G_{sm} (see Eq. 9), obtained by integrating the local measurements obtained by the optical probe and the net solids circulation rates, G_s, determined by the butterfly-valve closing method (see Liu, 2001) for 40 different operating conditions covering low to high solids flux conditions. In almost all cases, the difference between the two methods is less than 30%. The root-mean-square deviation is 22.8%, larger than one would wish, but acceptable in many gas–solids transport systems, especially when operated at high solids fluxes. However, it can be seen from Figure 13 that the optical-fiber probe usually gives a higher G_s than the butterfly-valve method. The bias factor between the two methods, defined as

$$F_m = \exp\left(\frac{1}{n}\sum_{i=1}^{n}\ln\left(\frac{G_{sm}}{G_s}\right)\right), \qquad (13)$$

is found to be 1.11, indicating that the integrated flux from the optical-fiber probe is 11% higher on average than that from the butterfly-valve method. The discrepancy is likely to arise from one or more of the following factors:

(1) Statistical fluctuations, caused by turbulent flow of the gas–particle suspensions, can cause errors when estimating particle transit times (see Part I) from cross-correlation peak positions (Lassahn and Baker, 1982).

(2) Each velocity value was obtained by cross-correlating signals over a very brief integration period (duration ~14.6 ms), yielding an "average" velocity over this brief period. As just analyzed, use of time–mean quantities tends to lead to overestimations of the actual flux. Averaging even over such a brief period can cause some overestimation of the solids flux.

(3) The butterfly-valve method is subject to error, for example, due to its finite closing time and disturbance of the loop caused by the extra pressure drop across the butterfly valve.

While it is impossible to state which of the two methods is subject to the greatest error, the bias is small enough that both can be considered to be reasonably accurate.

Nonisokinetic sampling probe

The radial profiles of local solids flux obtained by the optical-fiber probe are compared with those measured by the nonisokinetic sampling method in Figures 14 and 15. The sampling procedure and device were similar to those of Issangya (1998), except that the downward flux at the wall was determined by inverting the probe tip to face upwards and applying the same suction velocity as for the measurement of

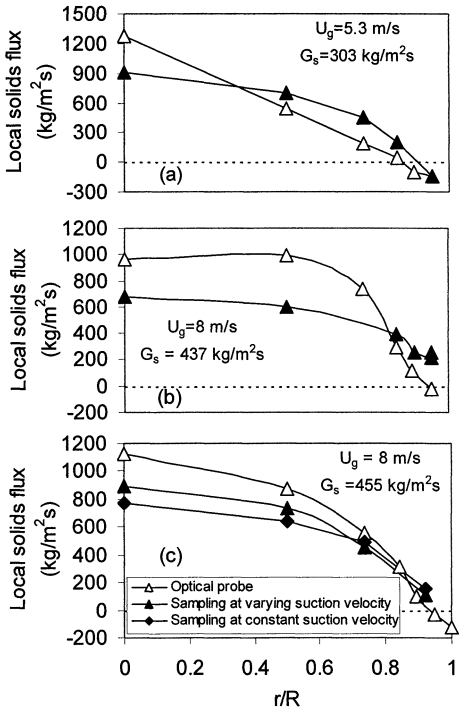

Figure 15. Comparison of radial profiles of local solids flux obtained by optical-fiber probe and nonisokinetic sampling probe at $z = 4.2$ m and various high-flux operating conditions.

Open symbols correspond to optical probe; closed symbols to suction probe.

upward flux. At intermediate net solids circulation fluxes (Figure 14) or low superficial gas velocities (Figure 15a), there is reasonable agreement between these two methods. However, for high-flux conditions (Figures 15b and 15c), the sampling method gives significantly lower fluxes in the core of the riser and higher fluxes in the wall region.

For the nonisokinetic method, the suction velocity was kept constant and approximately equal to the superficial gas velocity for all radial positions. As a result, the suction velocity is much lower than the local particle velocity for the central region and much higher in the wall region. Our experimental tests have shown that for suspensions denser than a few percent solids volume fraction, the measured flux increases with increasing suction velocity. This suggests that using the nonisokinetic suction probe method to measure the flux distribution in the high-density CFB can give a lower value in the riser interior, while leading to overestimation near the wall. This is supported by Figure 15c, where, when the suction velocity was adjusted to be closer to the local time–mean gas velocity (open triangles), the measured fluxes increased in the central region and decreased near the wall. The overall distribution was then closer to that obtained by the optical-fiber probe method.

The cross-sectional average solids fluxes measured by a nonisokinetic sampling probe are also compared in Figure 13 with those obtained by the optical probe and the butterfly-valve technique. It can be seen that all three measurement techniques give similar values for the conditions studied.

While it is again impossible to evaluate with certainty the exact errors in the two methods, we note that the optical-fiber probe is both less intrusive and better able to respond to rapid fluctuations than suction probes. As a result, Figures 14 and 15 provide an indication of the errors inherent in suction probe measurements.

Conclusion

The local instantaneous solids flux was determined by multiplying the simultaneously determined suspension density (local volume concentration times particle density) times the local instantaneous particle velocity of the same particles in a high-density circulating fluidized riser for FCC particles. The results are in reasonable agreement with those obtained by pressure transducers for apparent solids holdups, the butterfly-valve quick-closing technique for total solids circulation rates, and nonisokinetic sampling for local time–mean solids flux distribution. The probe provides an excellent means of obtaining simultaneous local instantaneous particle velocities, solids concentrations, and solids fluxes.

Except at the axis, instantaneous particle velocities and particle concentration are negatively correlated, with the strongest correlation occurring between the riser axis and the wall. Using the product of time–mean velocity and time–mean suspension density to estimate the local time–mean solids flux therefore leads to erroneous results.

Acknowledgment

Financial support from the Natural Sciences and Engineering Research Council of Canada (NSERC) is gratefully acknowledged.

Notation

c = local instantaneous solids volume fraction
$\bar{c}$ = time–mean local solids volume fraction
c' = fluctuating component of local solids volume fraction
c_m = time–mean cross-sectional average solids volume fraction
F_m = bias factor defined in Eq. 13
G_s = local instantaneous solids circulation flux, kg/m$^2\cdot$s
$\overline{G_s}$ = time–mean local solids flux, kg/m$^2\cdot$s
G_{sm} = time–mean cross-sectional average solids flux, kg/m$^2\cdot$s
$G_s(t)$ = instantaneous local solids flux, kg/m$^2\cdot$s
N = number of determinations
r = radial coordinate, m
R = radius of riser, m
T = cross-correlation integration time period, s
t = time, s
U_g = superficial gas velocity, m/s
$v_p, v_p(t)$ = instantaneous local particle velocity, m/s
v_{pm} = time–mean cross-sectional average particle velocity, m/s
$\overline{v_p}$ = time–mean local particle velocity, m/s
z = vertical coordinate, m

Greek letters

$\epsilon(r), \epsilon$ = instantaneous local voidage
$\bar{\epsilon}$ = time–mean local voidage
ϵ' = fluctuating component of local voidage
ϵ_m = riser cross-sectional average voidage
Φ_{Err} = error factor defined by Eq. 12
φ = dimensionless radial position, $= r/R$
ρ = density, kg/m^3

Subscripts

1,2 = data-acquisition channel 1, 2
g = gas
i = i^{th} determination
p = particle

Literature Cited

Arena, U. A., A. Cammarota, L. Massimilla, and D. Pirozzi, "The Hydrodynamic Behavior of Two Circulating Fluidized Bed Units of Different Sizes," *Circulating Fluidized Bed Technology*, Vol. II, P. Basu and J. F. Large, eds., Pergamon Press, Oxford, p. 223 (1988).

Bi, H. T., J. Zhou, S. Z. Qin, and J. R. Grace, "Annular Wall Layer Thickness in Circulating Fluidized Bed Risers," *Can. J. Chem. Eng.*, **74**, 811 (1996).

Issangya, A. S., J. R. Grace, D. Bai, and J. Zhu, "Further Measurements of Flow Dynamics in a High-Density Circulating Fluidized Bed Riser," *Powder Technol.*, **111**, 104 (2000).

Issangya, A. S., "Hydrodynamics of a High-Density Circulating Fluidized Bed," PhD Thesis, The Univ. of British Columbia, Vancouver, B.C., Canada (1998).

Jiang, P., and L.-S. Fan, "On the Turbulent Radial Transfer of Particles in a CFB Riser," *Fluidization*, Vol. IX, L. S. Fan and T. M. Knowlton, eds., Engineering Foundation, New York, p. 83 (1999).

Lassahn, G. D., and A. G. Baker, "Errors in Cross-Correlation Peak Location," *J. Dyn. Syst. Meas., Control, Trans. ASME*, **104**, 194 (1982).

Lin, J., J. R. Grace, and X. Bi, "Novel Multifunctional Optical-Fiber Probe: I. Development and Validation," *AIChE J.*, **49** (2003).

Liu, J., "Particle and Gas Dynamics in a High-Density Circulating Fluidized Bed," PhD Thesis, The Univ. of British Columbia, Vancouver, BC, Canada (2001).

Louge, M., and H. Chang, "Pressure and Voidage Gradients in Vertical Gas–Solid Risers," *Powder Technol.*, **60**, 197 (1990).

Qi, C., and I. Farag, "Lateral Particle Motion and Its Effect on Particle Concentration Distribution in the Riser of CFB," *AIChE Symp. Ser.*, **89**(296), 73 (1993).

Qian, G., and J. Li, "Particle-Velocity Measurement in CFB with an Integrated Probe," *Circulating Fluidized Bed Technology*, Vol. IV, A. A. Avidan, ed., AIChE, New York, p. 274 (1994).

Weinstein, H., and J. Li, "An Evaluation of the Actual Density in the Acceleration Section of Vertical Risers," *Powder Technol.*, **57**, 77 (1989).

Zhu, C., M. C. Slaughter, and S. L. Soo, "Covariance of Density and Velocity Fields of a Gas–Solids Suspension," *Rev. Sci. Instrum.*, **62**, 2835 (1991).

Manuscript received Feb. 4, 2002, and revision received Dec. 3, 2002.